C. R. Mecanique 347 (2019) 477–489

Contents lists available at ScienceDirect

Comptes Rendus Mecanique

www.sciencedirect.com

Effect of non-persistent joints distribution on shear behavior

Hang Lin [a,*], Xuran Ding [a], Rui Yong [b,*], Wanzhong Xu [c], Shigui Du [b]

[a] School of Resource Safety Engineering, Central South University, Changsha, Hunan 410083, China
[b] Ocean College, Zhejiang University, Zhoushan, Zhejiang 316000, China
[c] College of Territory and Resource Engineering, Kunming University of Science and Technology, Kunming, Yunan 650093, China

ARTICLE INFO

Article history:
Received 8 December 2018
Accepted 20 May 2019
Available online 3 June 2019

Keywords:
Non-persistent joints
Joints distribution type
Joint persistency
Numerical simulation
Shear strength

ABSTRACT

The particle flow code 2D (PFC2D) is used to establish a coplanar, non-persistent joint model. Three joint distribution types, namely, both-side (type a), scattered (type b), and central (type c), are set according to their position. Numerical simulations of the direct shear test are conducted to investigate the effect of non-persistent joint distribution and connectivity on shear mechanical behavior. Simulation results are in good agreement with the analytical solutions to Jennings' criterion, and show: (1) type-c and type-b joints have high strength, whereas type-a joints have low strength. Shear strength and modulus increase with a decrease in joint persistency, and the shear displacement that correspond to shear strength increases with a decrease in persistency. (2) The brittle failure characteristics of the sample are evident when the intact rock bridge area is large. Reinforcement at both ends of the joint limits shear deformation, and shear strength can be effectively improved when joint persistency is large. The small-area dispersed reinforcement joint method cannot effectively improve shear strength. (3) The comprehensive shear strength parameters and the shear strength of the non-persistent joints can be predicted well using Jennings' criterion. Cohesion is the dominant factor that controls shear strength.

1. Introduction

Jointed rock masses widely exist in nature, and most rock engineering instabilities are caused by joint failure [1–7]. Due to the existence of joints, the integrity of rock mass is destroyed, and its mechanical properties are affected because of joint failure. The occurrence, length, composition, and mechanical properties of joints significantly influence the safety and failure modes of rock masses [8]. Joint reinforcement can effectively improve the strength and stability of rock mass. Many theoretical, experimental, and numerical studies on persistent and non-persistent joints have been carried out [9–15]. Lajtai [16] divided the failure modes of intact rock bridges into three types, namely, tensile, shear, and ultimate, and proposed their respective failure criteria. Asadizadeh, Moosavi, Hossaini and Masoumi [17] conducted direct shear experiments on rock samples with different types of non-persistent joint and found that normal stress had the greatest influence on shear strength. Tang, Xia and Liu [18] proposed the modified Jennings' criterion by considering the weakening of mechanical parameters of rock bridges. Based on experiments and PFC numerical simulation, Ghazvinian [19] found that the failure mode

* Corresponding authors.
E-mail addresses: linhangabc@126.com (H. Lin), 244316889@qq.com (X. Ding), yongrui_usx@hotmail.com (R. Yong), xuwanzhongcsu@126.com (W. Xu), dushigui@126.com (S. Du).

https://doi.org/10.1016/j.crme.2019.05.001
1631-0721/

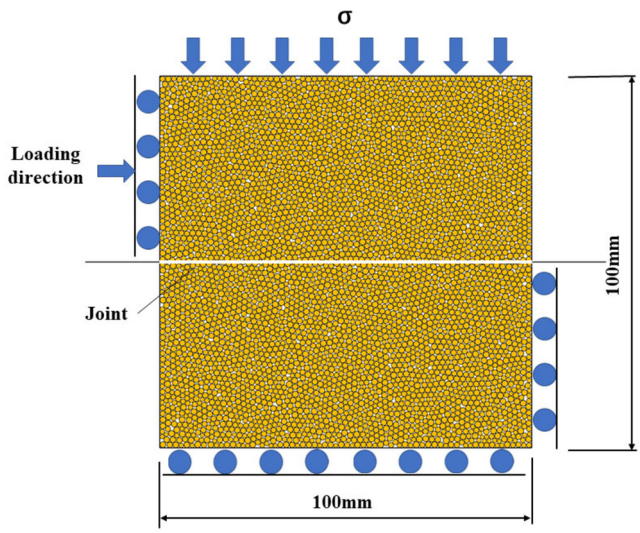

Fig. 1. Numerical model.

of a rock with non-persistent joints was mainly affected by joint persistency. Bahaaddini, Sharrock and Hebblewhite [9] used PFC3D to model the synthetic rock mass and investigated the mechanical properties of multiple sets of parallel discontinuities under uniaxial compression. Cheng, Yang and He [20] studied the influence of microscopic parameters on the direct shear strength of joint. At present, numerical simulations mainly focus on the crack propagation of discontinuous joints and the crack transfixion mode under different persistency values in compressive-shear test, whereas the joint distribution position needs to be examined to further understand the effect of the reinforcement position of persistent joints on their mechanical properties. Therefore, the particle flow code in two dimensions (PFC2D) was adopted in this study to investigate the shear mechanical behavior of non-persistent joints under different persistency and joint distribution types to achieve effective control over the joint surface.

2. Modeling

2.1. Numerical model

The discrete element method PFC was adopted to establish a numerical simulation model. PFC2D simulated the motion and interaction of the particle by using the discrete element method, which is widely used to study the mechanical properties of rocks and rock-like materials [21–24]. A 100 mm × 100 mm numerical model was established (Fig. 1). Different walls were generated to form the model shear boxes for the direct shear test, and the walls were divided into top and bottom groups. When the direct shear test is performed, the top part is applied to the right velocity and the bottom part remains at rest. The whole model is generated using 5030 particles, which has a specific porosity of 0.10, a density of 2020 kg/m^3, and a particle radius of 0.6–0.9 mm, and the particle diameter ratio (d_{max}/d_{min}) is 1.5. Fine river sand with a grain size of 0.5–1.0 mm was used to make intact rock samples for laboratory experiments, so particles with radius of 0.6 to 0.9 mm, within the range of 0.5–1.0 mm, were selected. Many studies were carried out using PFC2D with $d_{max}/d_{min} = 1.5$–2.0 (d is the particle diameter) [25–28]. In addition, when L/d (L is the smallest characteristic model length and d is the median particle size) is less than 50, the macroscopic property (such as Young's modulus, Poisson's ratio, and UCS) of the model exhibit a large variation, when L/d is greater than 50, the macroscopic properties of the model tend to be stable [29]. In this paper, d_{max}/d_{min} is 1.5 and $L/d = 133$, greater than 50, meets the requirements.

The contact between rock particles and particles is the linear parallel bond model, and the contact between particles and walls is the linear model. The parallel bond model has not only normal and shear stiffness, but also normal and shear strength. Parallel bonding contacts resist particle rotation. When the normal stress or shear stress exceeds the contact strength, the contact stiffness disappears. When the contact is tensile failure, the tensile strength becomes zero, while when the contact is shear failure, shear strength drops to the residual strength. The residual shear strength is related to the normal force (σ) and the friction coefficient (μ) [9]. Therefore, since the parallel bond model has the characteristics of simulating local damage and stiffness degradation caused by rock bond failure [30], the parallel bond model is adopted in the numerical model.

Three different joint distribution types, namely, both-side (type a), scattered (type b), and central (type c), were set to investigate the effect of the non-persistent joint distribution type on shear mechanical behavior (Fig. 2). Types a and b have two discontinuous joints, and type c has one continuous joint. Moreover, the sum of the joint lengths in the three cases is equal. The joint persistency factor was set as 0 (intact rock sample), 0.2, 0.4, 0.6, 0.8, and 1 (connected joint sample) to

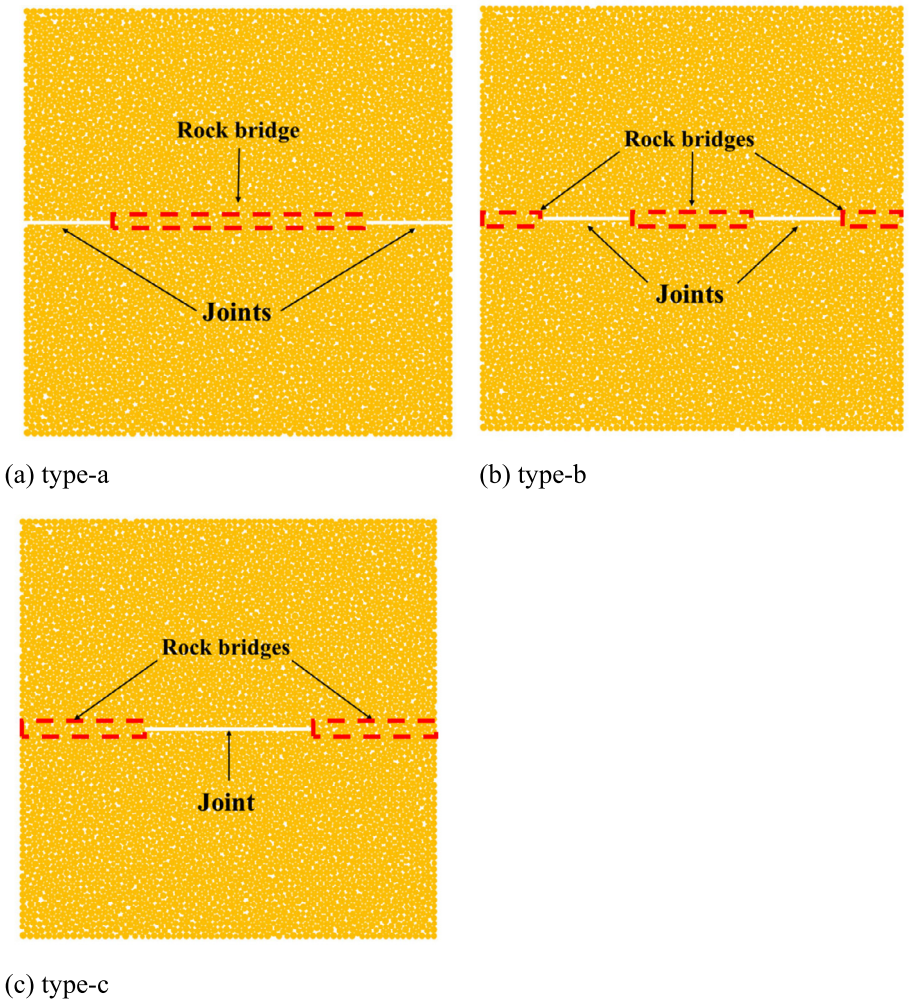

Fig. 2. Three types of joint distribution.

Table 1
Mechanical properties of the intact rock.

Uniaxial compressive strength (MPa)	Tensile strength (MPa)	Cohesion (MPa)	Internal angle of friction (°)	Elastic modulus (GPa)	Poisson's ratio
18.97	1.64	1.84	58.47	2.20	0.2

further study the effect of persistency on the shear mechanical behavior of discontinuous joints. In the direct shear process, the normal pressure is set at five levels: 0.5, 1.0, 1.5, 2.0, and 2.5 MPa.

2.2. Micro parameter calibration

Shear stress and shear displacement are recorded in the simulation process. The micro parameters were selected by matching the numerical simulation curves and laboratory test curves as the target through the trial calculation of the micro parameters. In the laboratory test, white Portland cement numbered 425 and fine river sand with a grain size of 0.5–1.0 mm were used to make intact rock samples at the upper and lower parts of the joints. Plaster and water were mixed in a weight ratio of 5:3. And the sample dimension was 100 mm × 100 mm. The shearing test equipment used is RYL-600, and the normal load is 100 N/s, the shear load being applied at the shear rate of 1 mm/min. The corresponding physical and mechanical parameters were obtained through compression and direct shear tests on the intact rock sample (Table 1). The joint test results are used as a reference for the micro parameter calibration because the proportion of mortar used in this study is similar to that used by Liu, Liu, Wang, Bo and Zhang [31]. The friction coefficient for the continuous joint is $f = 0.83$, and the cohesion is $c = 0.19$ MPa. Through trial calculation, the micro-parameters of rock can be obtained (Table 2). A comparison between numerical and experimental results is shown in Figs. 3–5. Matching PFC simulation curve

Table 2
Micro parameters of simulated numerical model.

Parameter types	Micro parameters	Value
Basic particle parameters	Density ρ (kg m^{-3})	2020
	Porosity P	0.10
	Particle radius ratio R_{max}/R_{min}	1.5
	Effective modulus E_c (GPa)	3.0
	Normal-to-shear stiffness ratio k_n/k_s	1.5
	Friction coefficient μ	5.5
Parameters of the linear parallel bond model	Bond effective modulus $\overline{E_c}$ (MPa)	10
	Normal-to-shear stiffness ratio $\overline{k_n}/\overline{k_s}$	2.2
	Tensile strength (MPa)	1.6
	Cohesion (MPa)	12.5
	Friction angle (°)	55.3
Parameters of the joint	Normal stiffness k_n (GPa)	20
	Shear stiffness k_s (GPa)	10
	Cohesion (MPa)	10
	Friction coefficient μ	4.0
	Tensile strength (MPa)	5
	Joint thickness (mm)	1.5

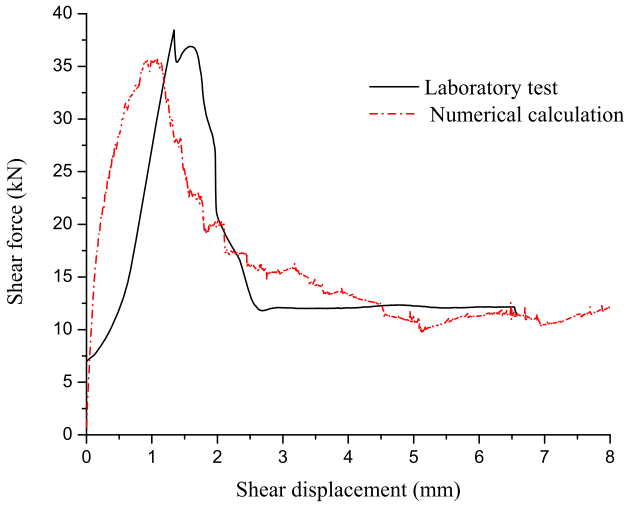

Fig. 3. Micro parameter calibration of an intact rock sample.

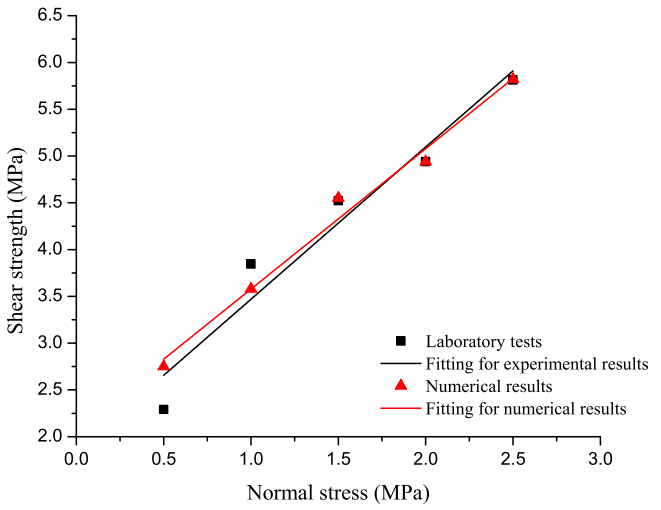

Fig. 4. Shear strength of rock obtained by laboratory test and numerical simulation.

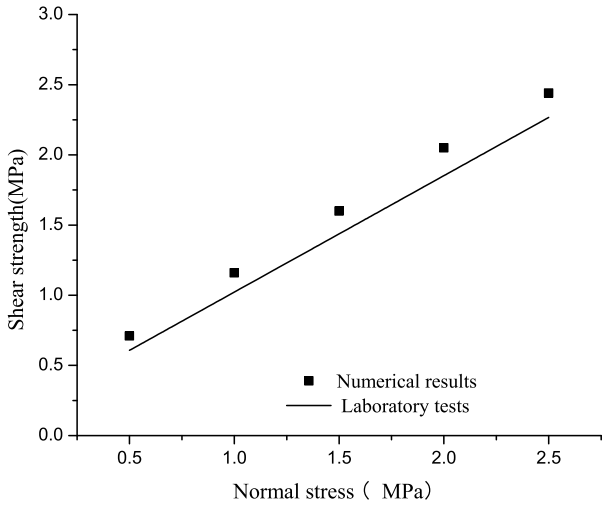

Fig. 5. Shear strength of persistent joint obtained by laboratory test and numerical calculation.

Table 3
Shear strength parameters obtained by laboratory test and numerical simulation.

	Intact rock		Joint	
	Cohesion *c* (MPa)	Internal angle of friction (°)	Cohesion *c* (MPa)	Internal angle of friction (°)
Laboratory test	1.84	58.47	0.19	39.69
Numerical simulation	2.08	56.31	0.29	41.02

and laboratory experiment curve, usually focusing on the peak strength, the residual strength, and the shear modulus of the two curves. Since the PFC particles' stiffness is a constant, the initial compaction stage of the physical experiment cannot be simulated, resulting in a large initial modulus. However, from Fig. 3, it can be seen that the pre-peak shear modulus, the peak strength, the strain softening rate, and the residual strength are well fitted by laboratory experiment. The shear stiffness of the laboratory test curve is 35.7 kN/mm, and that of the numerical simulation curve is 38 kN/mm. The shear strength parameters, the cohesion and internal friction angle were fitted on the basis of the Mohr–Coulomb criterion, showing that the numerical and experimental results are consistent (Table 3). Therefore, the mesoscopic parameter values of the numerical model are correct.

3. Calculation results and discussion

3.1. Effect of the joint distribution type on the shear stress–shear displacement relationship

The shear stress–shear displacement relationship of type-a,b,c joint specimens at the joint persistency of 0.4 is displayed in Fig. 6. The shear stress–shear displacement curve can be divided into linear–elastic, nonlinear–plastic, peak, strain softening, and residual stress stages. The comparison of the curves under different normal stresses shows that the slope of the curve at the stage of linear elasticity does not change with the normal stress, indicating that the normal load has minimal effect on the initial shear modulus. The shear displacement that corresponding to the initial point of the nonlinear plastic stage increases continuously with normal stress. Shear strength and residual stress increase with normal stress.

The effect of different joint distribution types on shear mechanical behavior is compared (Fig. 7). The type-b,c samples have high strength, whereas the type-a sample has low strength. The joints located at the shear load action (both side end) are more likely to crack because of shear action, which causes the damage on the entire sample, thereby resulting in low strength. The curves of the type-b,c specimens basically coincide before the peak value, and shear strength is roughly the same, indicating that, when the joint area is the same and the joint is not located at the shear-loading position, the cracking situation is roughly the same. Besides, the progressive joint closure under normal compression stress is classically managed (for cracked media) by the evolution of the aspect ratio under loading, whatever the (non-propagating) crack length. Therefore, the aspect ratio of the type-c joint distribution being half as small than the one of the two other types, it seems to get a greater stiffness.

The type-a curve is relatively gentle with large peak shear displacement and small post-peak stress softening rate, showing its ductile characteristics compared with those of the two other types. The type-c curve is sharper near the peak value, its peak shear displacement is smaller, and its post-peak stress softening rate is larger than those of the two other types. The reason is that the type-a joint is located at the shear end. At the initial loading stage, the joint can be easily cracked under

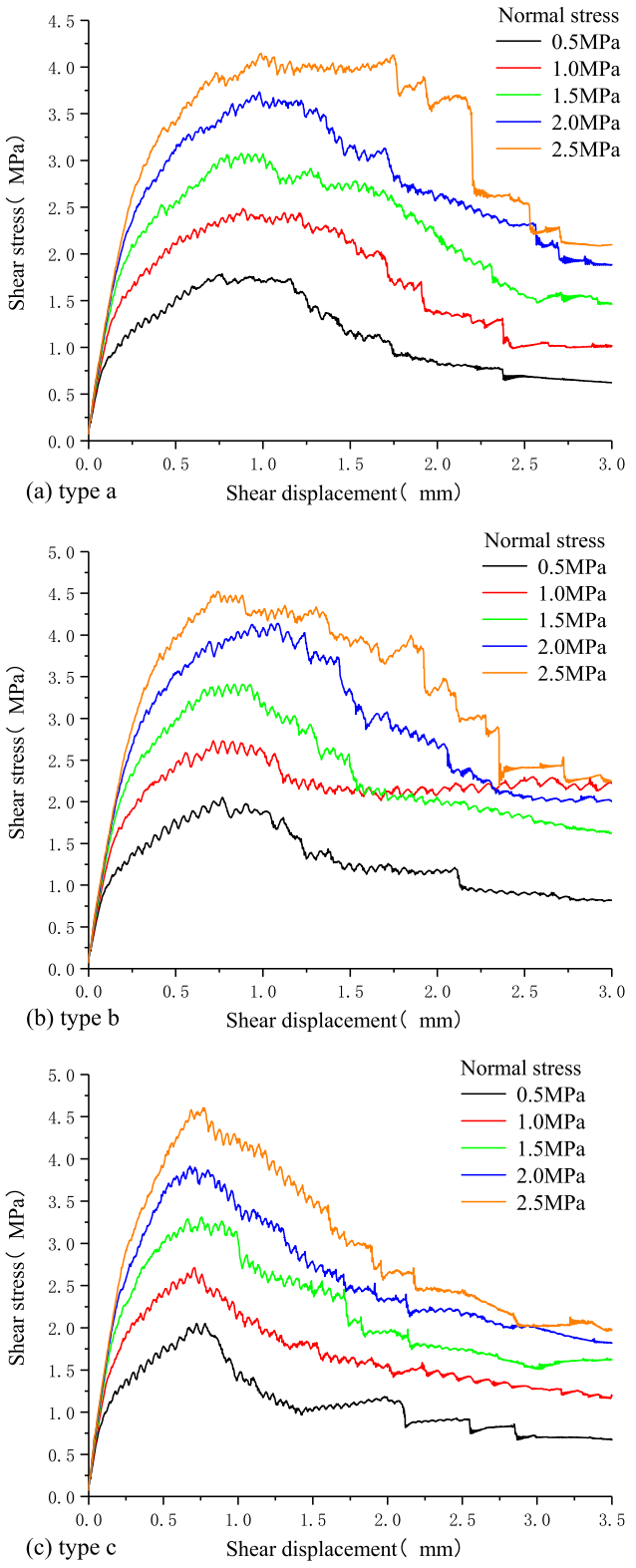

Fig. 6. Shear stress–shear displacement relations of joint specimens under different normal stresses.

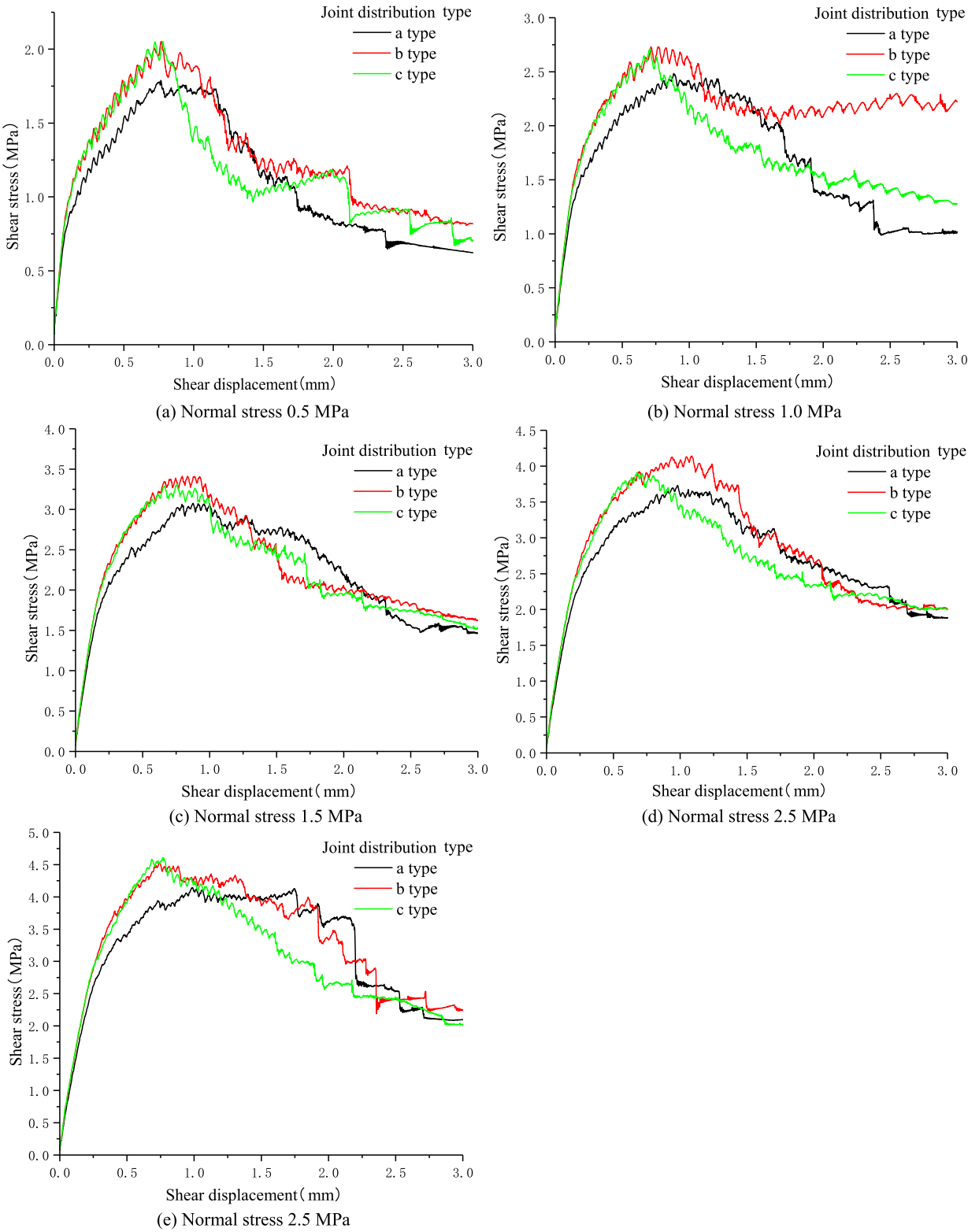

Fig. 7. Shear stress–shear displacement relationship of joint specimens under different distribution types.

the shear force to release the accumulated deformation energy. Therefore, the shear modulus is less than those of type-b,c samples. The type-c rock bridge constrains the deformation of the sample under loading. When the shear stress reaches its peak, the two rock bridges suddenly break and form a transfixion failure surface, accelerating the release of accumulated deformation energy. The type-b shear mechanical properties are observed between a and c. In addition, the residual strength is provided by the mechanical interaction and friction resistance of the failure surface. Therefore, the residual strengths of the three joint distribution types are basically the same.

3.2. Effect of joint persistency on the shear stress–shear displacement relationship

The normal stress of 1.5 MPa was set as an example to explore the effect of different joint persistency values on direct shear response. The corresponding shear stress and displacement curves were compared (Fig. 8). Shear strength and modulus increase with a decrease in joint persistency because when the latter decreases. Rock bridge has a constraint on shear displacement. The curve shape is flat and joint persistency is high when the joint shear strength peak to residual strength ratio is small. The test curve presents a linear yield shear curve when joint persistency is 1. At the initial loading stage, the shear displacement was small and linear segments were obvious. Subsequently, the joint surface begins to slide after the yield phase is reached. The larger the area of the rock bridge, the more the failure mode tends to intact rock shear failure, and the more obvious the brittle failure feature. At the same time, the shear displacement that corresponds to shear strength increases with a decrease in joint persistency because the area of the rock bridge is large. In addition, the failure surface of the joint is smooth, and the failure surface of the rock bridge is rough. Therefore, the lower the joint persistency is, the rougher the failure surface will be, the greater the mechanical interaction and friction resistance will be, thereby causing the mechanical interaction position to be prone to brittle failure and leading to a certain degree of stress drop, which is manifested as the sudden drop of post-peak stress. Therefore, a lower joint persistency leads to a larger residual strength of the sample and a larger fluctuation in the post-peak curve.

The effect of joint persistency on the shear strength analyzed (Fig. 9), where joint persistency 0 corresponds to the intact rock sample, and joint persistency 1 corresponds to the continuous joint sample. Their joint distribution types have no difference. Therefore, the three curves coincide at joint persistency 0 and 1. The peak value of shear strength increases linearly with normal stress. Under different joint persistency, the shear strength of type-c joint is larger than that of the other two types. If the continuous joint can effectively control the cracking, then it can improve the overall strength of the joint better. The strength of the type-b joint is relatively low, thereby indicating that the effect of dispersive reinforcement on continuous joints is relatively weak. Shear strength increases linearly with a decrease in joint persistency. It can be seen from the strength law of type c that, when joint persistency is high, strengthening at the end of joint can limit its deformation and effectively improve the shear strength of the joint surface. In type b, our results indicate that the shear strength of the joint could not be effectively improved by means of small area dispersive reinforcement in the continuous joint. Furthermore, the difference in strength between type-a and type-c joints is gradually reduced with persistency. When joint persistency is 0.2, the two are basically coincident, indicating that when the joint area is small, the joint distribution type has minimal effect on shear strength.

3.3. Effect of joint persistency and distribution on the shear mechanical parameters

Jennings' criterion has been widely used in engineering because it not only considers the strength of the rock bridge, but also those of the joints [32]. The shear strength parameters of the joints and of the intact rock bridges were linearly weighted so as to obtain the comprehensive shear strength parameters of the jointed rock. Moreover, its calculation formula is simple. The weighted average of the mechanical parameters of joints and rock bridges was adopted using Jennings' shear strength criteria to further describe the shear mechanical characteristics of non-persistent joints:

$$\eta = \frac{L_j}{(L_j + L_r)} \tag{1}$$

$$\tan\bar{\varphi} = \eta \tan\varphi_j + (1-\eta)\tan\varphi_0 \tag{2}$$

$$\bar{c} = \eta c_j + (1-\eta)c_0 \tag{3}$$

$$\tau = \eta(\sigma \tan\varphi_j + c_j) + (1-\eta)(\sigma \tan\varphi_0 + c_0) \tag{4}$$

where η is joint persistency; L_j and L_r are the lengths of the joint and of the rock bridge, respectively; c_j and φ_j are the shear strength parameters of the joint; c_0 and φ_0 are the shear strength parameters of the intact rock (rock bridge); $\bar{c}$ and $\bar{\varphi}$ are the comprehensive shear strength parameters, and τ is shear strength.

When the joint distribution type is unknown, the average shear strength of the three joint distribution types can be used to represent the shear strength of the joint, which is compared with Jennings' criterion (Fig. 10). The values calculated by Jennings' criterion agree well with the results of the numerical simulation, indicating that the shear strength of non-persistent joints can be remarkably predicted by using Jennings' criterion when only the joint persistency is known and the joint distribution type is unknown.

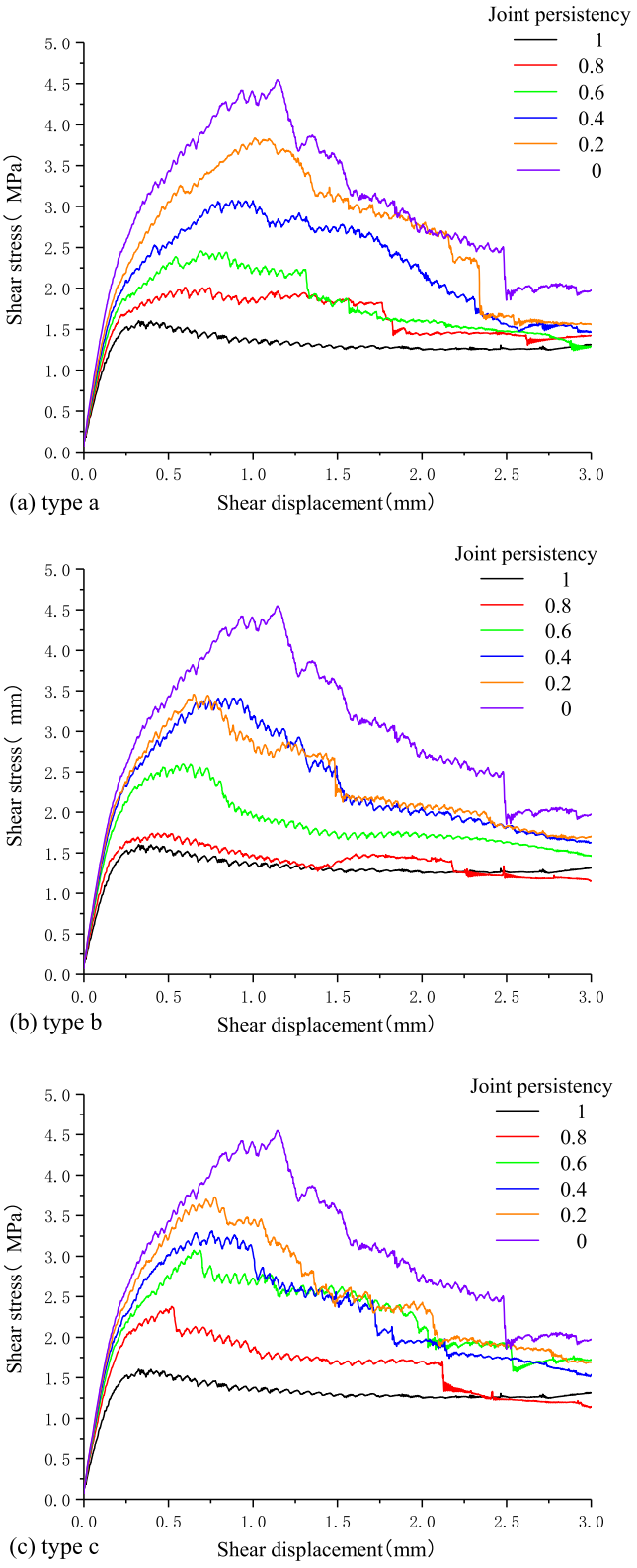

Fig. 8. Shear stress–shear displacement relations of joint samples under different persistency values.

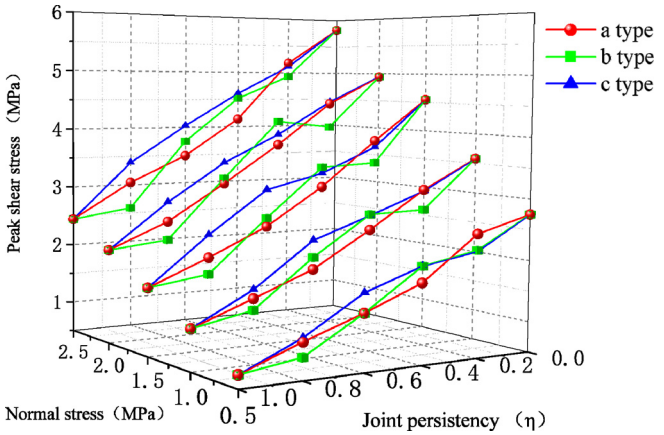

Fig. 9. Relationship between shear strength of joints and persistency and normal stress under different distribution types.

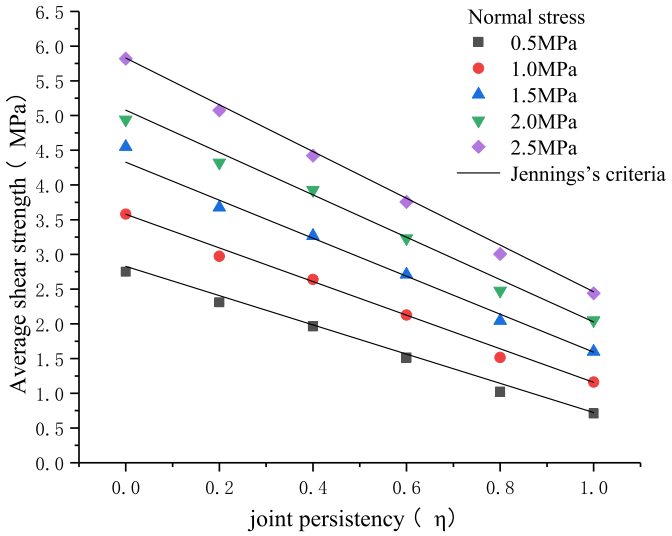

Fig. 10. Value of Jennings' criteria compared with the average shear strength of the joint.

The shear strength parameters can be obtained: the cohesion c and the friction coefficient $\tan\varphi$, and the average value of the shear strength parameters of the three joint distribution types, according to the relationship between normal stress and shear strength obtained by numerical simulations (Fig. 11 and 12). The shear strength parameters decrease with an increase in joint persistency, and the relationship between the two exhibits significant linear characteristics. The variation trend of cohesion with the joint persistency of the three joint distribution types is the same as the trend of the peak shear strength. The joint distribution type with high shear strength has large cohesion. When the persistency in the three joint types is 0.2, type a has the largest cohesion and the smallest friction coefficient, but the corresponding shear strength is the largest. Similar results are obtained in other cases of joint persistency, that is, cohesion is the dominant factor that controls shear strength, and shear strength is mainly affected by cohesion. Fig. 11 shows that the average values of cohesion are in good agreement with the values calculated by Jennings' criterion (Eq. (2)), thereby indicating that Jennings' criterion (Eq. (2)) can help evaluate the equivalent cohesion of the non-persistent joint surface.

Fig. 12 shows the relations of three types of friction coefficients. The friction coefficient of type c is larger and above the average value. The friction coefficient is obtained by linear fitting, which is roughly the same as the calculation result of Jennings criterion. When $\eta = 0.8$, the friction coefficient of type-b and type-c joints has a large deviation. But, in general, with an increase in persistency, the friction coefficients of the three types decrease. Besides, type c is the most sensitive one to normal load, and its shear strength increases with normal load at the highest rate. Type-a is the least sensitive. Joints can be compacted under normal load and produce normal deformation because they have certain thickness and poor mechanical properties relative to rock. Therefore, the normal load of the joint plane is mainly borne by a rock bridge. The stress conditions of joint and rock bridge are similar to that of a bridge, that is, the joint is comparable to a bridge span, and the rock bridge corresponds to the pier. When the rock bridge area is small, the reaction force of the rock bridge against the normal load can be approximated as the concentrated force. Thus, the simplified analysis of the stress condition of the

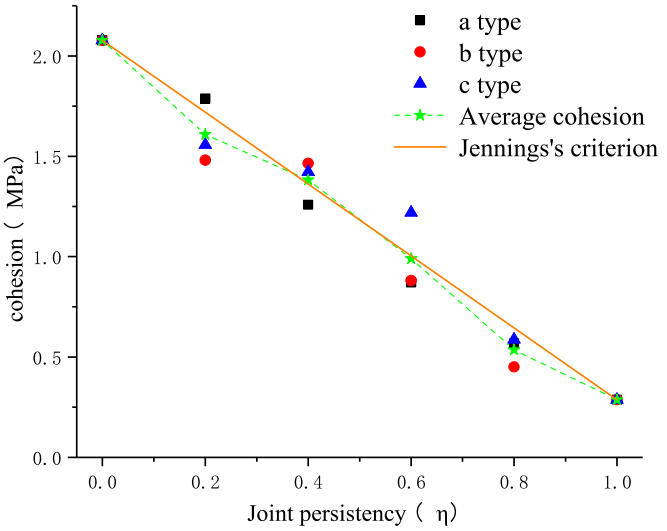

Fig. 11. Joint cohesion changes with persistency.

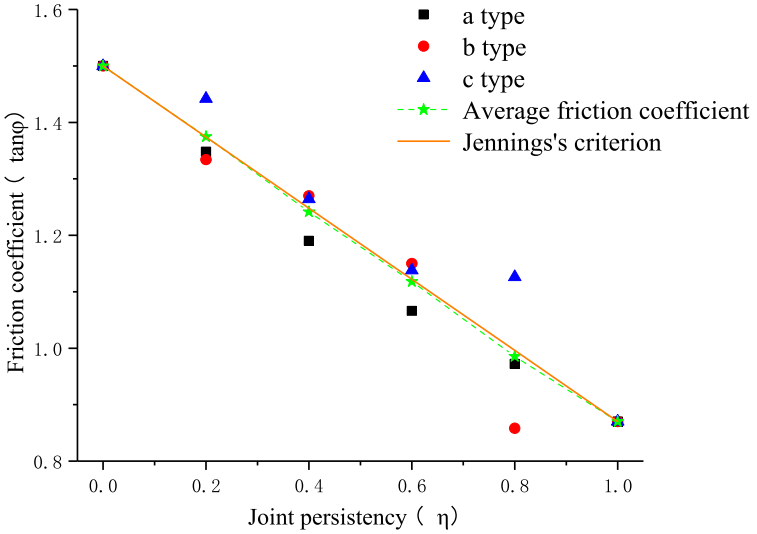

Fig. 12. Joint friction coefficient changes with connectivity.

shear plane under high joint persistency is carried out. When the joint is at the end of the shear plane, the end portion is a free end, and when the rock bridge is at the end of the shear plane, the end portion is regarded as a normal hinged point. The stress condition and moment are shown in Fig. 13. The maximum moment of types a- and c occurs in the rock bridge part, whereas the maximum moment of type c occurs in the joint part. Therefore, the type-c upper and lower surfaces of joints are more likely to be compacted and generate greater friction resistance in shear, thereby resulting in a larger friction coefficient of type-c joints.

4. Conclusions

(1) Shear strength and modulus increase with decreasing joint persistency. The failure pattern tends to shear failure of the intact rock, and the brittle failure characteristics becomes obvious when the rock bridge area is large. The shear displacement that corresponds to shear strength increases with decreasing joint persistency. Under the same normal load, the failure surface will be rough, and the mechanical interaction and friction will increase when the joint persistency is small. Moreover, brittle fracture is more likely to occur at the position of mechanical interaction, thereby resulting in a stress drop, which is the sudden drop of shear stress after a peak.

(2) If the cracking can be controlled effectively, then the strength of the non-persistent jointed rock mass can be improved. When the joint persistency is high, reinforcing the joint end can limit its deformation and effectively improve the

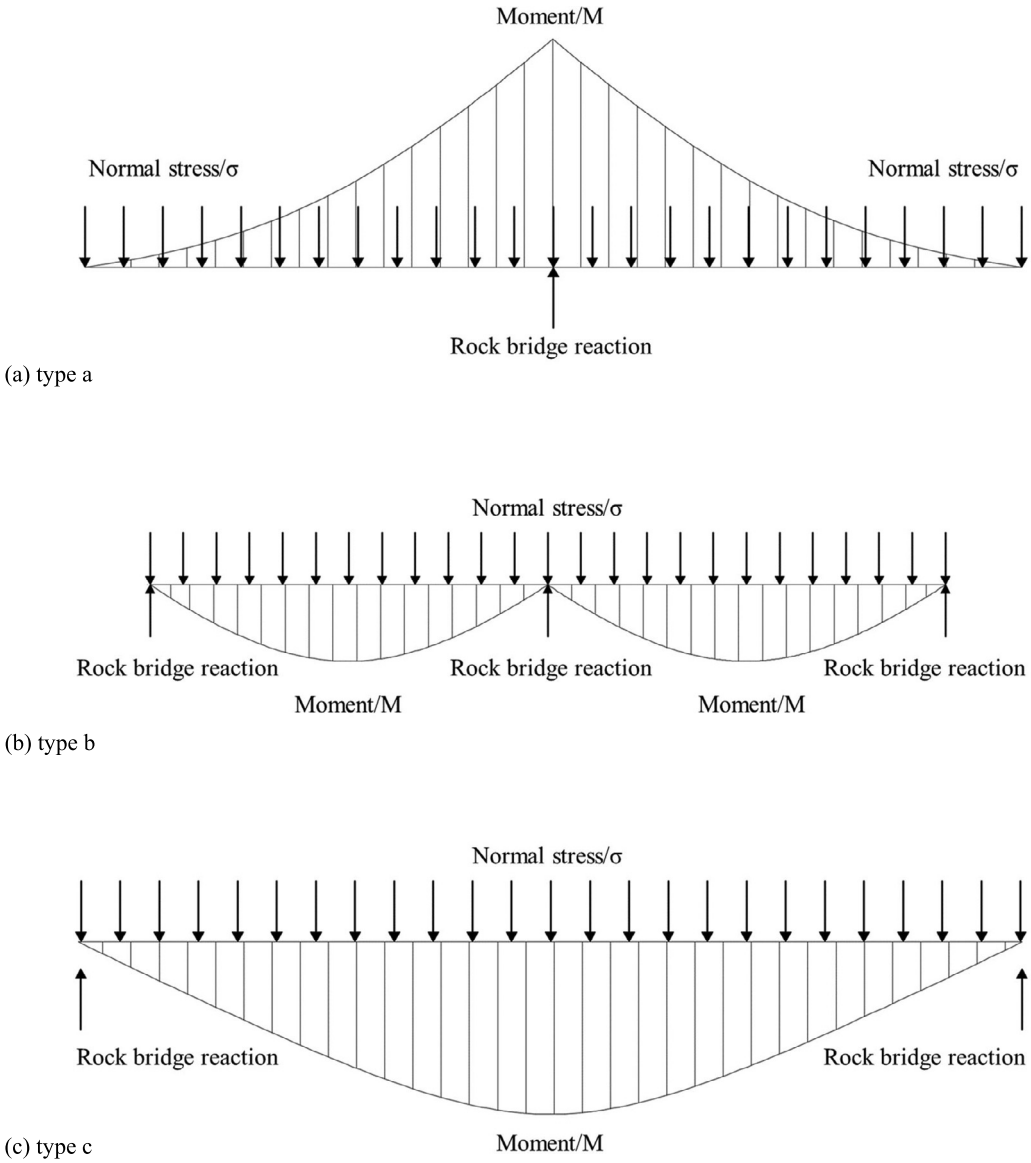

Fig. 13. Schematic of the stress condition and the moment of shear plane.

shear strength of the joint surface. The shear strength of continuous joints cannot be effectively increased by small area dispersion reinforcement. Jennings' criteria and numerical simulation results are in good agreement. Jennings' criterion can be used to evaluate the shear strength of non-persistent joints and the comprehensive shear strength parameters on the shear plane.

(3) Jennings' criterion did not consider the influence of water. Therefore, in this paper, only dry conditions were simulated. To consider the role of water, PFC needs to be combined with other methods. The influence of fluid pressure on the mechanical behavior of discontinuous joints will be further studied in the future.

Acknowledgements

This paper was funded by projects Nos. 51774322 and 41562016 supported by the National Natural Science Foundation of China, by project No. 2018JJ2500 supported by the Hunan Provincial Natural Science Foundation of China. The authors wish to acknowledge these supports. The anonymous reviewer is gratefully acknowledged for his/her valuable comments on the manuscript.

References

[1] X. Fan, P.H.S.W. Kulatilake, X. Chen, Mechanical behavior of rock-like jointed blocks with multi-non-persistent joints under uniaxial loading: a particle mechanics approach, Eng. Geol. 190 (2015) 17–32.
[2] Y. Zhao, L. Zhang, W. Wang, et al., Cracking and stress–strain behavior of rock-like material containing two flaws under uniaxial compression, Rock Mech. Rock Eng. 49 (7) (2016) 2665–2687.
[3] S.Q. Yang, X.R. Liu, H.W. Jing, Experimental investigation on fracture coalescence behavior of red sandstone containing two unparallel fissures under uniaxial compression, Int. J. Rock Mech. Min. Sci. 63 (5) (2013) 82–92.
[4] N. Halakatevakis, A.I. Sofianos, Correlation of the Hoek–Brown failure criterion for a sparsely jointed rock mass with an extended plane of weakness theory, Int. J. Rock Mech. Min. Sci. 47 (7) (2010) 1166–1179.
[5] A. Haque, J. Kodikara, A simplified analytical model for predicting the shear behaviour of regular triangular rock/concrete joints under constant normal stiffness, Geotechnique 62 (2) (2012) 171–176.
[6] J. Shen, M. Karakus, Three-dimensional numerical analysis for rock slope stability using shear strength reduction method, Can. Geotech. J. 51 (2014) 164–172.
[7] Y. Wang, H. Lin, Y. Zhao, Analysis of fracturing characteristics of unconfined rock plate under edge-on impact loading, Eur. J. Environ. Civ. En. (2019) 1–16.
[8] R. Yong, J. Ye, B. Li, et al., Determining the maximum sampling interval in rock joint roughness measurements using Fourier series, Int. J. Rock Mech. Min. Sci. 101 (2018) 78–88.
[9] M. Bahaaddini, G. Sharrock, B.K. Hebblewhite, Numerical investigation of the effect of joint geometrical parameters on the mechanical properties of a non-persistent jointed rock mass under uniaxial compression, Comput. Geotech. 49 (20) (2013) 206–225.
[10] N. Bahrani, P.K. Kaiser, B. Valley, Distinct element method simulation of an analogue for a highly interlocked, non-persistently jointed rockmass, Int. J. Rock Mech. Min. Sci. 71 (1) (2014) 117–130.
[11] D.L. Hopkins, The implications of joint deformation in analyzing the properties and behavior of fractured rock masses, underground excavations, and faults, Int. J. Rock Mech. Min. Sci. 37 (1–2) (2000) 175–202.
[12] W.G. Pariseau, S. Puri, S.C. Schmelter, A new model for effects of impersistent joint sets on rock slope stability, Int. J. Rock Mech. Min. Sci. 45 (2) (2008) 122–131.
[13] H. Lin, H. Wang, X. Fan, et al., Particle size distribution effects on deformation properties of graded aggregate base under cyclic loading, Eur. J. Environ. Civ. En. 23 (3) (2019) 269–286.
[14] R. Yong, X. Fu, M. Huang, et al., A rapid field measurement method for the determination of Joint Roughness Coefficient of large rock joint surfaces, KSCE J. Civ. Eng. 22 (1) (2018) 101–109.
[15] Q. Liu, W. Xing, Y. Li, Numerical built-in method for the nonlinear JRC/JCS model in rock joint, Sci. World J. 2014 (8) (2014) 735497.
[16] E.Z. Lajtai, Shear strength of weakness planes in rock, Int. J. Rock Mech. Min. Sci. Geomech. Abstr. 6 (5) (1969) 499–515.
[17] M. Asadizadeh, M. Moosavi, M.F. Hossaini, et al., Shear strength and cracking process of non-persistent jointed rocks: an extensive experimental investigation, Rock Mech. Rock Eng. 51 (2) (2018) 415–428.
[18] Z.C. Tang, C.C. Xia, Y.M. Liu, Modified Jennings shear strength criterion based on mechanical weakening model of rock bridges, Chin. J. Geotechn. Eng. 34 (11) (2012) 2093–2099.
[19] A. Ghazvinian, A study of the failure mechanism of planar non-persistent open joints using PFC2D, Rock Mech. Rock Eng. 45 (5) (2012) 677–693.
[20] Y. Cheng, W. Yang, D. He, Influence of structural plane microscopic parameters on direct shear strength, Adv. Civ. Eng. 2018 (2018) 9178140.
[21] R. Cao, P. Cao, H. Lin, et al., Experimental and numerical study of the failure process and energy mechanisms of rock-like materials containing cross un-persistent joints under uniaxial compression, PLoS ONE 12 (12) (2017) e0188646.
[22] R. Cao, W. Tang, H. Lin, et al., Numerical analysis for the progressive failure of binary-medium interface under shearing, Adv. Civ. Eng. (2018) 4197172.
[23] A. Manouchehrian, M. Sharifzadeh, M.F. Marji, et al., A bonded particle model for analysis of the flaw orientation effect on crack propagation mechanism in brittle materials under compression, Arch. Civ. Mech. Eng. 14 (1) (2014) 40–52.
[24] R.-H. Cao, P. Cao, H. Lin, et al., Failure characteristics of intermittent fissures under a compressive-shear test: experimental and numerical analyses, Theor. Appl. Fract. Mech. 96 (2018) 740–757.
[25] H. Huang, Discrete Element Modeling of Tool-Rock Interaction, Ph.D. thesis, University of Minnesota, MN, USA, 1999.
[26] D.O. Potyondy, P.A. Cundall, A bonded-particle model for rock, Int. J. Rock Mech. Min. Sci. 41 (8) (2004) 1329–1364.
[27] B. Yang, J. Yue, S. Lei, A study on the effects of microparameters on macroproperties for specimens created by bonded particles, Eng. Comput. 23 (6) (2006) 607–631.
[28] J. Yoon, Application of experimental design and optimization to PFC model calibration in uniaxial compression simulation, Int. J. Rock Mech. Min. Sci. 44 (6) (2007) 871–889.
[29] X. Ding, L. Zhang, H. Zhu, et al., Effect of model scale and particle size distribution on PFC3D simulation results, Rock Mech. Rock Eng. 47 (6) (2014) 2139–2156.
[30] R.H. Cao, P. Cao, H. Lin, et al., Particle flow analysis of direct shear tests on joints with different roughnesses, Rock Soil Mech. 34 (2013) 456–463.
[31] S.G. Liu, H.N. Liu, S.J. Wang, et al., Direct shear tests and PFC2D numerical simulation of intermittent joints, Chin. J. Rock Mech. Eng. 27 (9) (2008) 1828–1836.
[32] B. Stimpson, Failure of slopes containing discontinuous planar joints, in: Proc 19th US Symposium on Rock Mechanics, Stateline, NV, USA, University of Nevada, Reno, NV, USA, 1978, pp. 296–300.